Cryo-EM structure of a 3D DNA-origami object

Xiao-chen Bai[a], Thomas G. Martin[b], Sjors H. W. Scheres[a,1], and Hendrik Dietz[b,1]

[a]Medical Research Council Laboratory of Molecular Biology, Cambridge CB2 0QH, United Kingdom; and [b]Physics Department, Walter Schottky Institute, Technische Universität München, 85748 Garching near Munich, Germany

A key goal for nanotechnology is to design synthetic objects that may ultimately achieve functionalities known today only from natural macromolecular complexes. Molecular self-assembly with DNA has shown potential for creating user-defined 3D scaffolds, but the level of attainable positional accuracy has been unclear. Here we report the cryo-EM structure and a full pseudoatomic model of a discrete DNA object that is almost twice the size of a prokaryotic ribosome. The structure provides a variety of stable, previously undescribed DNA topologies for future use in nanotechnology and experimental evidence that discrete 3D DNA scaffolds allow the positioning of user-defined structural motifs with an accuracy that is similar to that observed in natural macromolecules. Thereby, our results indicate an attractive route to fabricate nanoscale devices that achieve complex functionalities by DNA-templated design steered by structural feedback.

Natural macromolecular machines have complex 3D shapes with subnanometer-precise structural features that enable executing tasks such as signal transduction, molecular transport, and enzymatic catalysis (1). A key goal for nanotechnology is to fabricate synthetic objects with similarly precise features to ultimately control tasks known today only from natural "nanomachines." Molecular self-assembly with DNA is considered a candidate route to achieve this goal (2–13). Densely packed 3D DNA-origami objects (14–18) seem particularly suited for use as rigid scaffolds to position reactive groups at target locations in space, and to implement features known from natural macromolecular complexes, such as shape complementarity and controlled domain movement. Designing such objects to meet precise structural specifications will benefit strongly from detailed 3D structural feedback. Here we present a cryo-EM map of an asymmetric, densely packed DNA object that comprises 15,238 nt in 164 chains. Combined with prior knowledge about the topology of chain connectivity, this map provided sufficient detail to construct a full pseudoatomic model for this particle. Thereby, our results provide structural feedback on DNA-templated design that will prove valuable for the design of complex functionalities.

Results and Discussion

DNA-Templated Design and Synthesis. Our DNA object was designed to be suitable for structure determination by cryo-EM single-particle analysis, because the choice of a distinctly asymmetric shape facilitated the recognition of different particle orientations in electron micrographs (Fig. 1A). The object was designed to assemble as 82 parallel dsDNA helices of varying length in a square lattice (17) of 10 columns and 12 rows and comprising a total of 15,238 nt with a molecular mass of 4.8 MDa (Fig. S1). A total of 740 nt were distributed among flexible loops at the ends of the helices to prevent aggregation by blunt-end stacking (19). Synthesis of the object was based on templated molecular self-assembly (3) with a 7,249-nt-long "scaffold" DNA strand derived from M13 bacteriophage and 163 shorter "staple" strands (Table S1). The object formed overnight in a one-pot reaction with high yield and few byproducts, such as higher-molecular-weight aggregates. It was purified from excess staple strands by molecular-weight cutoff filtration, which yielded particle solutions free from nucleic acid stains and gel matrix residues (Fig. S2).

Cryo-EM Single-Particle Analysis and Model Generation. Imaging of the sample by cryo-EM revealed monodisperse particles with the expected dimensions and shape (Fig. S3). The particles showed suitable contrast in ice and adopted multiple orientations on the supporting continuous carbon film (Figs. 1 B and C). This allowed us to calculate a 3D reconstruction (20) from 28,502 individual particles with an overall resolution of 11.5 Å (Fig. S4). The resolution of the map varies with position, with an estimated range of 9.7 Å at the core to 14 Å at the periphery (Fig. 1D; *Materials and Methods*). With the exception of a region comprising helices in row 11 at the periphery of the object and a single cross-over in row 10, all helices and connecting cross-overs are well resolved in the map. The global shape of the reconstructed density is in agreement with the designed topology of the object. The overall dimensions of the object and the extent of global twist that results from a mismatch of B-form DNA helicity and the imposed square-lattice packing also agree with a prediction (21, 22) when using 2.6-nm effective helix diameter and 10.44 bp/turn reciprocal twist density (17) (Fig. S5).

Aided by knowledge of the designed topology of the 164 strands in the object, we constructed an initial atomic model that consisted of canonical B-form DNA segments (23) for all expected dsDNA helices and cross-overs. Flexible fitting of this model inside the cryo-EM density (24) yielded a pseudoatomic model for the entire object (Fig. 2 and Movie S1), except for the single-stranded loops at the boundaries, for which no density was observed. Throughout the object, the fitted model is in good agreement with the cryo-EM density, and nearly all residues form expected base pairs. Note that in the EM density, connections between neighboring helices are often visible at positions that do not coincide with covalent strand cross-over (Fig. 3 A–C), suggesting additional contacts beyond the two covalent strand cross-overs. However, low-pass filtering of our model to the same resolution as the EM map shows similar contacts (Fig. S6), indicating that the additional connections are due to the limited resolution of our map. The quality of the pseudoatomic model is highest at the core of the object, where it reproduces the observed major and minor grooves resolved in the map (Fig. 3B). According to the frequency-dependent decay of the power in our EM reconstruction (25), the rmsd of the atoms at the core of the object was estimated to be in the range of 2–3 Å (*SI Text*), thus providing experimental evidence that structural order that approaches that of natural nanomachines may be attained in discrete DNA objects.

Fig. 1. Cryo-EM reconstruction of a designed, densely packed DNA object. (*A*) Schematic representation of the designed rectangular lattice comprising 82 parallel dsDNA helices (gray circles). (*B*) Representative part of an electron micrograph. (Scale bar, 50 nm.) (*C*) Reference-free 2D class averages. (*D*) Six orthogonal views of the 3D reconstruction, shown as iso-density surface at density level 0.1.

Analysis of Structural Features. The pseudoatomic model enables the type of geometrical analysis required for designing objects with precise structural specifications. For example, in agreement with default B-form DNA geometry, we find that the average distance from base pair to base pair midpoints is 3.35 Å as derived from the helical distance between consecutive cross-overs that are resolved in the cryo-EM density. The design of the object assumes parallel double helices packed on a square lattice. Although the cross-sectional square lattice is indeed realized, we find that the helices are not parallel: on either side of the majority of cross-overs they enclose a nonzero angle within, but also out of the plane normal to the cross-over direction (Figs. 1*D* and 3 *A*–*D*). Globally, this results in a 3D chickenwire-like pattern whereby individual dsDNA helices form diamond-shaped cavities in between cross-overs (Fig. 3 *E* and *F*). The 3D chickenwire pattern is also correlated with an unusual geometry of the 377 Holliday junctions that connect the helices in the object (Fig. 3 *G* and *H*). As established by FRET (26, 27) and atomic force microscopy (AFM) measurements (28), Holliday junctions adopt stacked conformations in the presence of cations where the two opposite helices are at an angle γ of ∼60°. In crystal structures, Holliday junctions show similar features (29–31). However, both the in-plane and the out-of-plane bending that we find in our structure is absent in the crystal structures and was also not resolved in the FRET and AFM measurements. Moreover, the junctions in our object exhibit a left-handed, rather than a right-handed, interhelical conformation (Fig. S7). These large conformational differences suggest that Holliday junctions are easily deformed by any ordering scheme, be it through crystal contacts or scaffolding interactions inside a densely packed

DNA object. In the light of these results, future design of DNA objects to more precise structural specifications will benefit from the consideration of more appropriate cross-over models (Fig. 3 *I* and *J*).

We designed the termini of the 163 linear strands in the object to be mainly located 2 or 3 base pairs away from cross-overs. The termini result in covalent phosphodiester backbone nicks in dsDNA helices. We hypothesized that Holliday junction cross-overs with such nearby nicks might not fully form or that nicked helices might differ in shape from nonnicked helices. Our map reveals that this is not the case. Cross-overs with nearby nicks do not differ in geometry from nonnicked cross-overs (Fig. 3*H*). We also did not observe systematic differences when comparing nicked and nonnicked dsDNA helical stretches in the map. In addition, we investigated whether the nature of the local sequences at DNA cross-over positions leads to discernible differences in cross-over shape but could find no evidence for this.

Previously Unobserved DNA Topologies. The cryo-EM map also provides structural insights into a library of highly unusual DNA topologies, some of which can only exist because of the scaffolding provided by the densely packed design. In row 4, columns 4–9 of the object, we created a vertical stack of five Holliday junctions (Fig. 4*A*; Fig. 3*A* shows a vertical stack of three Holliday junctions). This motif is stabilized only by the stacking of base pairs at the junctions in addition to two covalent phosphodiester bonds at either end of the junction stack. In our map this motif is well resolved, thus pointing at a surprisingly high degree of structural order, contrary to what one might have intuited. We speculate that the systematic use of many of these junction stacks in future
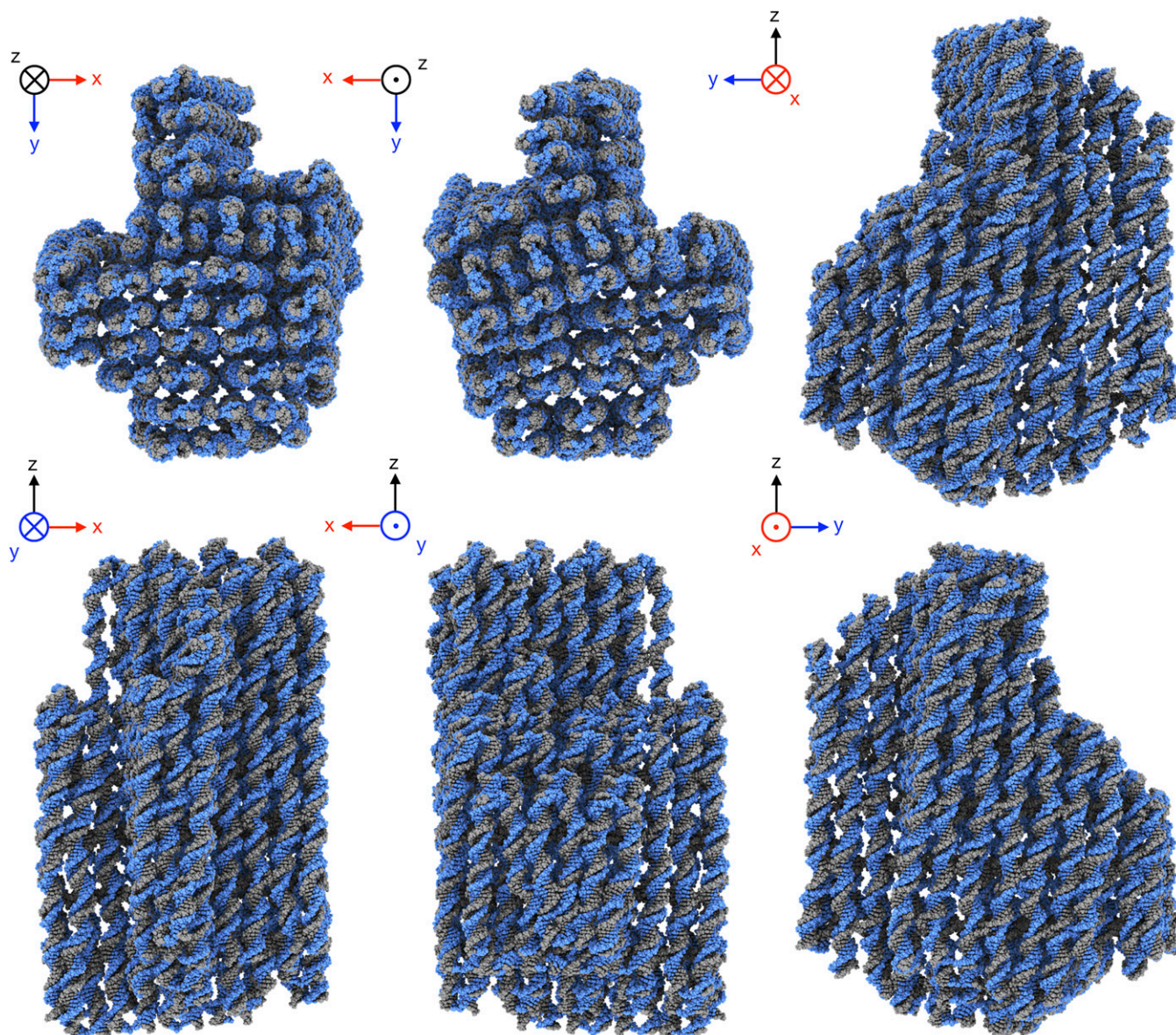
Fig. 2. Pseudoatomic model. Six orthogonal views of the pseudoatomic model that was fitted into the EM density map.

designs will lead to compaction and confer increased mechanical rigidity. In row 6, columns 1–6, we created a motif (Fig. 4*B*) that may be considered as a synthetic pseudohelix in which one strand follows a left-handed helical path with base pairs pointing along the helical direction, rather than orthogonally to the helical axis as in B-form dsDNA. The left-handed pseudohelix is stabilized by six short counter-strands of only 5- or 6-nt length. Again, the motif is well resolved in the EM density, albeit with less resolution because this motif occurs at the more flexible periphery of the object. In row 7, column 6, we omitted a single DNA base pair, which leads to a mismatch in backbone orientation at a cross-over to a neighboring helix in column 7. Previously, the introduction of many such omissions was used to design globally curved structures (15). In our map, a single base pair omission already results in a well-resolved bending deformation of both helices and a cross-over direction rotation (Fig. 4*C*), confirming that fine-tuning at the level of individual base pairs may afford precise control over orientation and location of structural features. Finally, column 0 is illustrative for how custom crevices may be created by rationally distributing cross-

overs, because dsDNA helices tend to splay away from each other in the absence of stabilizing cross-overs between them (Fig. 4*D*).

Conclusions

Our results demonstrate that designed, densely packed DNA objects are amenable to detailed structural characterization and may provide near atomic-level positional control. The range of topological motifs in our structure illustrates the versatility of DNA as a material for nanotechnology and highlights the existence of many unexplored design options for creating richer, more complex, but also more precise objects. Thereby, our results support a perspective in which chemical motifs may be arranged with precise structural specifications through an iterative strategy of DNA-templated design and 3D structural feedback. By using chemical groups attached to DNA strands or even reactive motifs formed by DNA itself, this strategy offers an attractive route to achieving complex functionalities known today only from natural nanomachines.
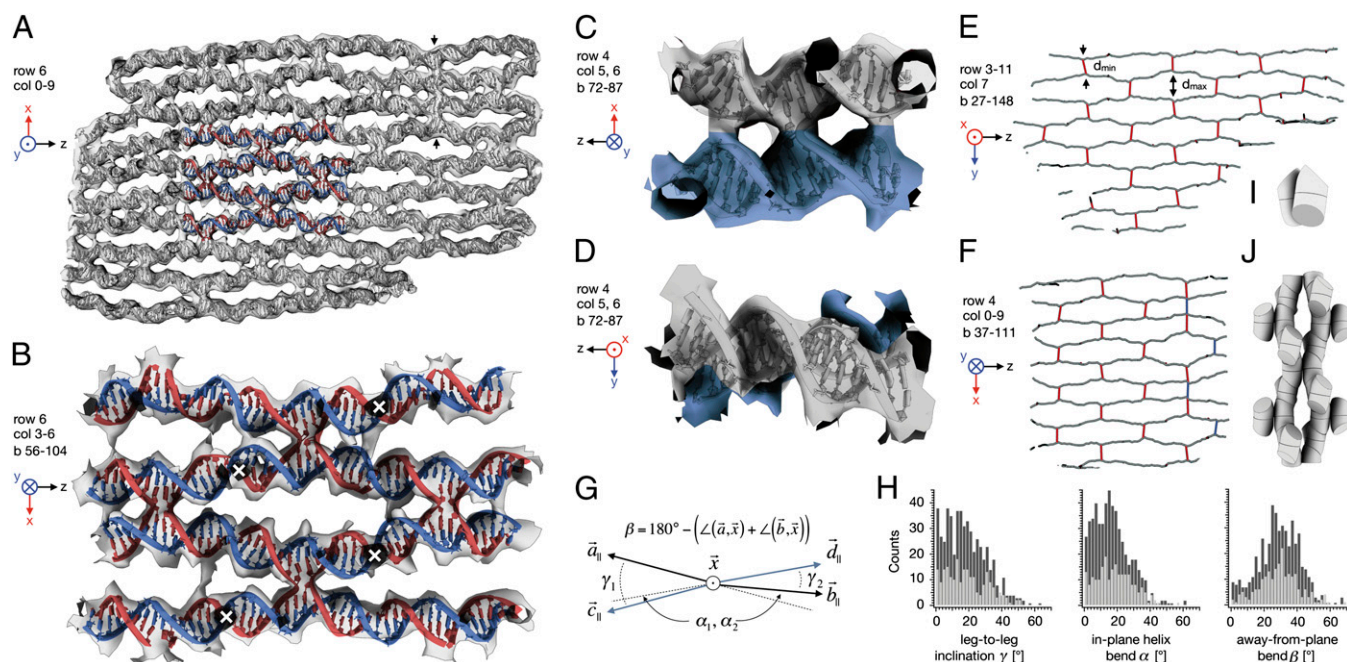
Fig. 3. Analysis of internal geometry. (*A*) Central slice through the object at row 6, showing the cryo-EM density map (transparent gray) and the fitted pseudoatomic model as ribbon/slab model. For part of the model, the scaffold is shown in blue and the staples in red. Vertical arrows indicate a vertical stack of three cross-overs. (*B*) Close-up of colored area in *A*, but rotated around the *z* axis by 180°. White crosses indicate out-of-plane cross-over positions. (*C*) Side view of a single cross-over. (*D*) Top view of the same cross-over as in *C*. (*E* and *F*) Schematic representation of the 3D chickenwire-like pattern found in the structure, depicting dsDNA helical stretches in gray and cross-overs in red. The pattern was computed using the coordinates of base pair midpoints in the pseudoatomic model. The midpoints of neighboring dsDNA helices move on average from a minimum distance $<d_{min}> = 18.5$ Å at the cross-over to a maximum distance of $<d_{max}> = 36$ Å away from each other. Cross-overs marked in blue indicate scaffold-based strand cross-overs. (*G*) Definition of the angles enclosed by the four helical legs of a cross-over. Vectors are computed using the coordinates of base pair midpoints at the cross-over position and 2 bp away from the cross-over in each leg. The cross-over vector x is computed from the coordinates of the midpoints between the two base pairs in each of the two helices at the cross-over position and is normal to what we call the cross-over plane. The subscript "$\parallel$" indicates vectorial projections into the cross-over plane. The angle β is also computed as indicated for vectors *C* and *D*. (*H*) Observed distribution of angles between the legs for cross-overs with (light gray) and without (dark gray) nearby nicks for 377 cross-overs in the structure, where each cross-over contributed two γ, α, and β angle values each. (*I*) Schematic representation of a revised cross-over model for DNA nanostructure design. (*J*) 3D chickenwire-like pattern formed by multiple instances of the revised cross-over model when rotated and translated according to the square-lattice packing connectivity scheme.

Materials and Methods

DNA-Templated Design and Synthesis. Our object was designed in iterative cycles of using caDNAno v0.2 (16) for strand routing and CanDo (21, 22) for estimation of rigidity and global twist. DNA scaffold strands were prepared as previously described (32). DNA staple oligonucleotide strands (Table S1) were prepared by solid-phase chemical synthesis (Eurofins MWG) with Eurofins MWG high purity salt free purification grade. The objects were synthesized in a one-pot mixture containing 20 nM 7,249-bases-long M13mp18 phage DNA, 200 nM oligonucleotide staple in a pH = 8 buffer that included 5 mM Tris·base, 1 mM EDTA, 20 mM MgCl2, and 5 mM NaCl. The mixture was incubated at 65 °C for 15 min, then annealed from 56 °C to 44 °C over the course of 12 h, and then stored at 4 °C. Analysis of the reaction products by agarose gel electrophoresis (Fig. S2) showed that the object assembled with high yield with negligible formation of byproducts. Purification from excess staple strands could therefore be performed using simple molecular weight cutoff filtration using 100 kDa Amicon filters (Millipore).

Electron Cryo-Microscopy. The purified sample at a concentration of ~10 nM in 10 mM Tris buffer (pH 7.6) with 20 mM MgCl2, 5 mM NaCl, and 1 mM EDTA was heated in a water bath at 37 °C for 1 h before preparing the grids to resolve multimers formed by blunt-end stacking. Aliquots of 3 μL were incubated for 3 min on glow-discharged holey carbon grids with an ultrathin carbon film on top (Agar Scientific, catalog no. S187-4), blotted, and plunge-frozen in liquid ethane using a Vitrobot (FEI Company). Grids were transferred to an FEI Polara G2 microscope that was operated at 300 kV. Images were recorded on a back-thinned FEI Falcon detector at a calibrated magnification of 42,277× (yielding a pixel size of 3.55 Å). The defocus was varied from 1 to 4 μm, using a dose of ~10 or 20 e−/Å². Electron micrographs were evaluated for astigmatism and drift, and 456 micrographs were selected for further analysis.

Image Processing. Contrast transfer function parameters were estimated using CTFFIND3 (33), and 28,502 particles were selected manually using the boxer program in the EMAN package (34). Reference-free 2D class averages and 3D reconstructions were calculated using RELION (20). The initial model for 3D refinement was calculated using CanDo (21). To avoid model bias against false high-resolution features, the initial model was low-pass filtered to 60 Å before refinement. The data set was split into two separate halves at the outset of refinement, and two independent models were refined simultaneously. This procedure allowed us to prevent overfitting and thereby obtain a reliable estimate of the resolution based on so-called "gold-standard" Fourier shell correlation (FSC) (35). The overall resolution of the final model was estimated to be 11.5 Å, based on the FSC = 0.143 criterion (35) (Fig. S4*A*). Low-pass filtering of the atomic model to the same resolution yielded a density map with similar features as the ones observed in our experimental map.

Inspection revealed that the density at the core of the object showed more high-resolution features than at the periphery. FSC calculations that used soft masks at different positions throughout the object indicated that the resolution varied from 9.7 Å at the core to ~14 Å at the periphery. To optimally represent the information content throughout the object, we calculated a composite map by low-pass filtering a sharpened map (with a B-factor of −2,000 Å²) at different resolution cut-offs in the range of 10–14 Å and combining these maps, depending on the estimated resolution at each position.

We confirmed the overall correctness of our structure by performing tilt-pair validation (36) (Fig. S4*B*). Using similar grids and microscope settings as the ones described above, 50 pairs of images were recorded at tilt angles of 0° and 10°, from which 342 particle pairs were selected manually. Alignment of the particles against the final composite map and analysis of the tilt-pair transformations were performed in the XMIPP package (37). Apart from
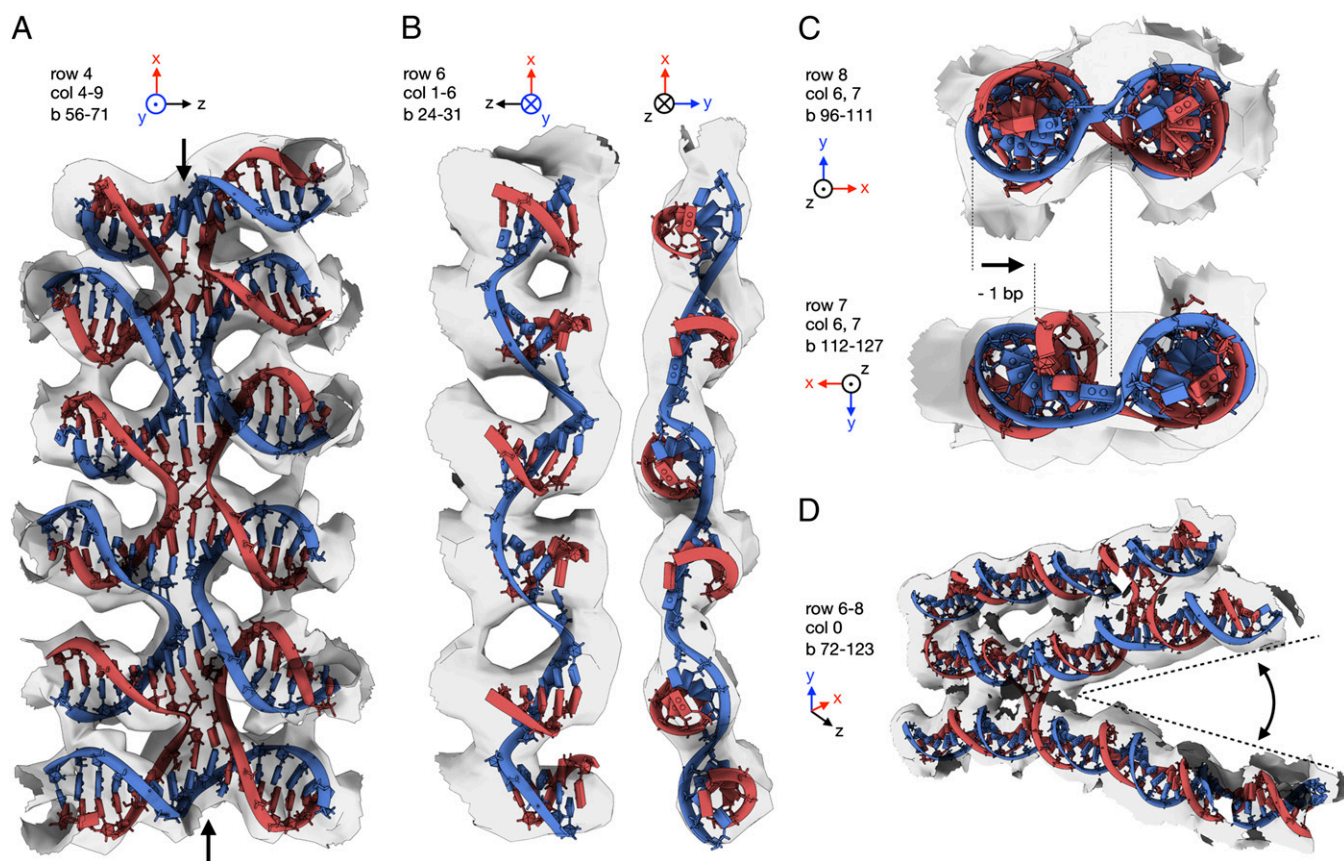
Fig. 4. Motifs beyond B-form DNA for nanotechnology. (*A*) A vertical stack of five Holliday junctions. (*B*) A pseudohelical structure that runs along the direction of the base pairs. (*C*) A bent helix and distorted cross-over due to an omitted base pair (*Lower*) and a typical cross-over without omission (*Upper*). (*D*) Crevices formed by splayed-out helices due to the absence of stabilizing cross-overs.

validating our map, this analysis also indicated that the individual particles may be aligned with an accuracy of ~2°.

Model Building. An initial atomic model with the designed topology of parallel dsDNA helices in a rectangular lattice and with the known nucleotide sequence was calculated using custom software that relied on 3DNA (23) to calculate canonical B-DNA for all designed helical fragments. Separate rigid body fitting of each of the 82 helices in the EM density map yielded a model that was suitable for flexible fitting using MDFF (24). Because the MDFF approach was not capable of handling the entire structure (which, including hydrogens, consists of 460,641 atoms), we split the structure into multiple substructures, consisting of three neighboring columns of the rectangular lattice each. Before molecular dynamics (MD) simulation, the geometry of these models was improved by up to 5,000 steps of energy minimization, which included hydrogen bond restraints but did not include restraints toward the EM density. Subsequent MD simulations were performed at 300 K for 200,000 steps using both hydrogen bond and dihedral angle restraints and a weight on the EM density (GSCALE) of 0.3 kcal/mol. After MD, another 2,000 steps of energy minimization were performed

using hydrogen bonds and dihedral restraints and a weight on the EM density of 1.0 kcal/mol. A final model for the entire object was obtained by combining the central columns of all substructures. Low-pass filtering of the atomic model density yielded a map with similar features as the ones observed in the experimental reconstruction (Fig. S6 *A and B*). Additionally, FSC calculations between the final model and the reconstruction showed significant correlation up to 12 Å, indicating that the quality of the atomic model reflects the quality of the reconstructed density (Fig. S6C).

1. Alberts B, et al. (2002) *Molecular Biology of the Cell* (Garland Science, New York).
2. Seeman NC (2010) Nanomaterials based on DNA. *Annu Rev Biochem* 79:65–87.
3. Rothemund PWK (2006) Folding DNA to create nanoscale shapes and patterns. *Nature* 440(7082):297–302.
4. Shih WM, Quispe JD, Joyce GF (2004) A 1.7-kilobase single-stranded DNA that folds into a nanoscale octahedron. *Nature* 427(6975):618–621.
5. Zheng J, et al. (2009) From molecular to macroscopic via the rational design of a self-assembled 3D DNA crystal. *Nature* 461(7260):74–77.
6. Han D, et al. (2011) DNA origami with complex curvatures in three-dimensional space. *Science* 332(6027):342–346.
7. Yurke B, Turberfield AJ, Mills AP, Jr., Simmel FC, Neumann JL (2000) A DNA-fuelled molecular machine made of DNA. *Nature* 406(6796):605–608.
8. Omabegho T, Sha R, Seeman NC (2009) A bipedal DNA Brownian motor with co-ordinated legs. *Science* 324(5923):67–71.
9. Wickham SF, et al. (2012) A DNA-based molecular motor that can navigate a network of tracks. *Nat Nanotechnol* 7(3):169–173.
10. Zhang C, et al. (2012) DNA-directed three-dimensional protein organization. *Angew Chem Int Ed Engl* 51(14):3382–3385.
11. Andersen ES, et al. (2009) Self-assembly of a nanoscale DNA box with a controllable lid. *Nature* 459(7243):73–76.
12. Voigt NV, et al. (2010) Single-molecule chemical reactions on DNA origami. *Nat Nanotechnol* 5(3):200–203.
13. Kato T, Goodman RP, Erben CM, Turberfield AJ, Namba K (2009) High-resolution structural analysis of a DNA nanostructure by cryoEM. *Nano Lett* 9(7):2747–2750.
14. Douglas SM, et al. (2009) Self-assembly of DNA into nanoscale three-dimensional shapes. *Nature* 459(7245):414–418.
15. Dietz H, Douglas SM, Shih WM (2009) Folding DNA into twisted and curved nanoscale shapes. *Science* 325(5941):725–730.

16. Douglas SM, et al. (2009) Rapid prototyping of 3D DNA-origami shapes with caDNAno. *Nucleic Acids Res* 37(15):5001–5006.
17. Ke Y, et al. (2009) Multilayer DNA origami packed on a square lattice. *J Am Chem Soc* 131(43):15903–15908.
18. Ke Y, Voigt NV, Gothelf KV, Shih WM (2012) Multilayer DNA origami packed on hexagonal and hybrid lattices. *J Am Chem Soc* 134(3):1770–1774.
19. Woo S, Rothemund PWK (2011) Programmable molecular recognition based on the geometry of DNA nanostructures. *Nat Chem* 3(8):620–627.
20. Scheres SH (2012) A Bayesian view on cryo-EM structure determination. *J Mol Biol* 415(2):406–418.
21. Castro CE, et al. (2011) A primer to scaffolded DNA origami. *Nat Methods* 8(3):221–229.
22. Kim DN, Kilchherr F, Dietz H, Bathe M (2012) Quantitative prediction of 3D solution shape and flexibility of nucleic acid nanostructures. *Nucleic Acids Res* 40(7):2862–2868.
23. Lu XJ, Olson WK (2003) 3DNA: A software package for the analysis, rebuilding and visualization of three-dimensional nucleic acid structures. *Nucleic Acids Res* 31(17):5108–5121.
24. Trabuco LG, Villa E, Mitra K, Frank J, Schulten K (2008) Flexible fitting of atomic structures into electron microscopy maps using molecular dynamics. *Structure* 16(5):673–683.
25. Henderson R, et al. (2011) Tilt-pair analysis of images from a range of different specimens in single-particle electron cryomicroscopy. *J Mol Biol* 413(5):1028–1046.
26. Murchie AI, et al. (1989) Fluorescence energy transfer shows that the four-way DNA junction is a right-handed cross of antiparallel molecules. *Nature* 341(6244):763–766.
27. Eis PS, Millar DP (1993) Conformational distributions of a four-way DNA junction revealed by time-resolved fluorescence resonance energy transfer. *Biochemistry* 32(50):13852–13860.
28. Mao C, Sun W, Seeman NC (1999) Designed two-dimensional DNA Holliday junction arrays visualized by atomic force microscopy. *J Am Chem Soc* 121:5437–5443.
29. Ortiz-Lombardía M, et al. (1999) Crystal structure of a DNA Holliday junction. *Nat Struct Biol* 6(10):913–917.
30. Nowakowski J, Shim PJ, Prasad GS, Stout CD, Joyce GF (1999) Crystal structure of an 82-nucleotide RNA-DNA complex formed by the 10-23 DNA enzyme. *Nat Struct Biol* 6(2):151–156.
31. Eichman BF, Vargason JM, Mooers BH, Ho PS (2000) The Holliday junction in an inverted repeat DNA sequence: Sequence effects on the structure of four-way junctions. *Proc Natl Acad Sci USA* 97(8):3971–3976.
32. Douglas SM, Chou JJ, Shih WM (2007) DNA-nanotube-induced alignment of membrane proteins for NMR structure determination. *Proc Natl Acad Sci USA* 104(16):6644–6648.
33. Mindell JA, Grigorieff N (2003) Accurate determination of local defocus and specimen tilt in electron microscopy. *J Struct Biol* 142(3):334–347.
34. Ludtke SJ, Baldwin PR, Chiu W (1999) EMAN: Semiautomated software for high-resolution single-particle reconstructions. *J Struct Biol* 128(1):82–97.
35. Scheres SHW, Chen S (2012) Prevention of overfitting in cryo-EM structure determination. *Nat Methods* 9(9):853–854.
36. Rosenthal PB, Henderson R (2003) Optimal determination of particle orientation, absolute hand, and contrast loss in single-particle electron cryomicroscopy. *J Mol Biol* 333(4):721–745.
37. Scheres SHW, Núñez-Ramírez R, Sorzano COS, Carazo JM, Marabini R (2008) Image processing for electron microscopy single-particle analysis using XMIPP. *Nat Protoc* 3(6):977–990.

Supporting Information

Bai et al. 10.1073/pnas.1215713109

SI Text

The frequency-dependent fall-off of signal power in a cryo-EM reconstruction may be used to estimate the intrinsic variability in the underlying structure. After correcting for the modulation transfer function of the detector, a B-factor sharpening of approximately $-1{,}000$ Å^2 gave a density map at the core of the object, as expected from the atomic model. This B-factor still comprises various components, among which errors in the rotational and translational assignments and intrinsic variability in the structure are assumed to be the most significant ones. From the tilt-pair validation plot in Fig. S4, we estimated the errors in the rotational assignments to be on the order of 2°. According to Henderson et al. (1) this estimate results in a B-factor component

of $B_{rot} = (\Delta\Theta \, D)^2/2200 = \sim400$ Å^2. On the basis of signal-to-noise considerations, we estimated the errors in the translational assignments to be on the order of ~0.5 pixel, or ~1.8 Å, leading to a B-factor component of $B_{trans} = 8 \, \pi^2 \, (\text{rmsd})^2 = 250$ Å^2. That then leaves a remaining B-factor component for the intrinsic structural variability (at the core of the object) of $B_{structural} = 1{,}000 - 400 - 250 = 350$ Å^2, which corresponds to an rmsd in the atom positions of ~2 Å. The mentioned range of up to 3 Å in the main text is an attempt to reflect uncertainties in our B-factor estimation and in the empirical calculations related to the orientational errors. Additionally, as mentioned in the main text, the structural variability is larger at the periphery of the object than at its core.

1. Henderson R, et al. (2011) Tilt-pair analysis of images from a range of different specimens in single-particle electron cryomicroscopy. *J Mol Biol* 413(5):1028–1046.

Fig. S1. caDNAno object design diagram. Scaffold strand path is depicted with black lines, and staple strands are shown as red lines.
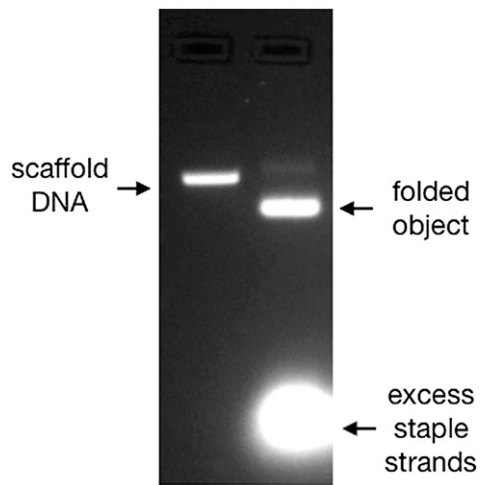
Fig. S2. Gel electrophoretic folding quality assessment. Photograph of an ethidium bromide-stained 2% agarose gel on which reaction products were electrophoresed.
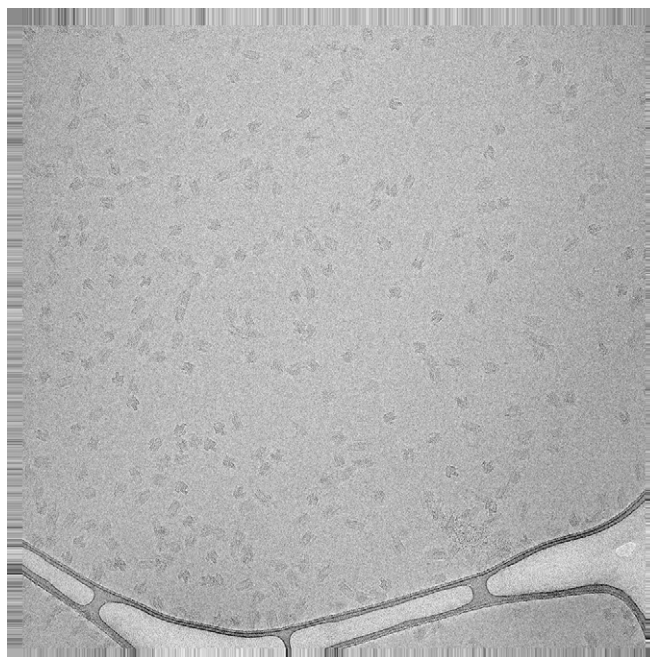
Fig. S3. Exemplary cryo-EM micrograph. The field of view is 1.45 μm × 1.45 μm.
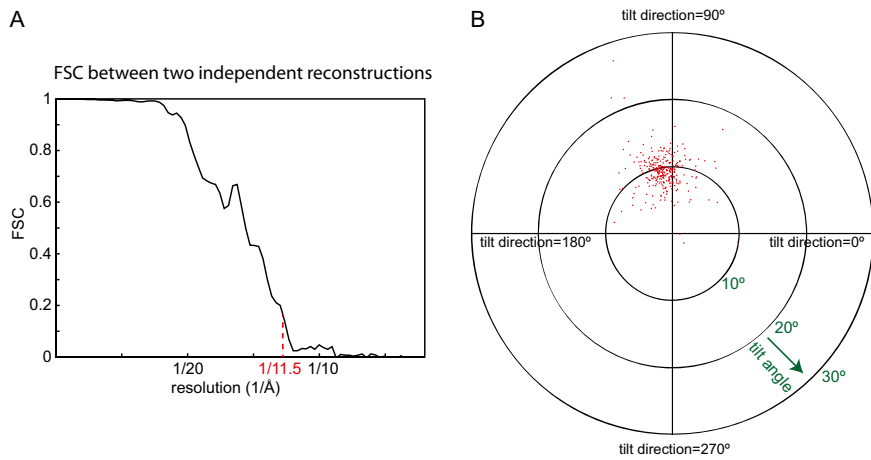
Fig. S4. Quality assessment of the cryo-EM map. (*A*) Fourier shell correlation (FSC) curve. (*B*) Tilt-pair validation plot. Note that 32 of the 342 particle pairs had tilt differences larger than 30° and are therefore not depicted.
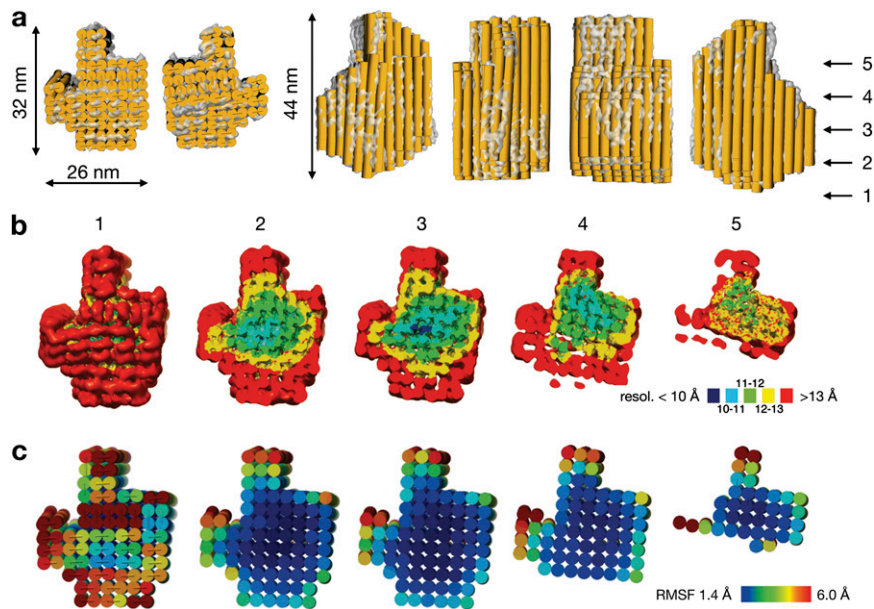
Fig. S5. Comparison of cryo-EM map and CanDo predictions. (*A*) Cryo-EM map (gray) and CanDo predicted shape (ocre) agree in overall dimensions and twist when assuming a reciprocal twist density of 10.44 bp/turn and an effective helical diameter of 2.6 nm. (*B* and *C*) The variation in resolution as estimated in the cryo-EM map (*B*) and the estimated root mean square fluctuation (rmsf) of the atoms in the shape prediction (*C*). Cross-sections are shown at five different slices (1–5) through the object, the positions of which are indicated with vertical arrows in *A*. Note that CanDo does not output a color scale bar for the estimated rmsf values. The scale bar shown reflects that colors are reported to range from dark blue (for an rmsf of 1.4 Å) to dark red (for an rmsf of 6 Å).
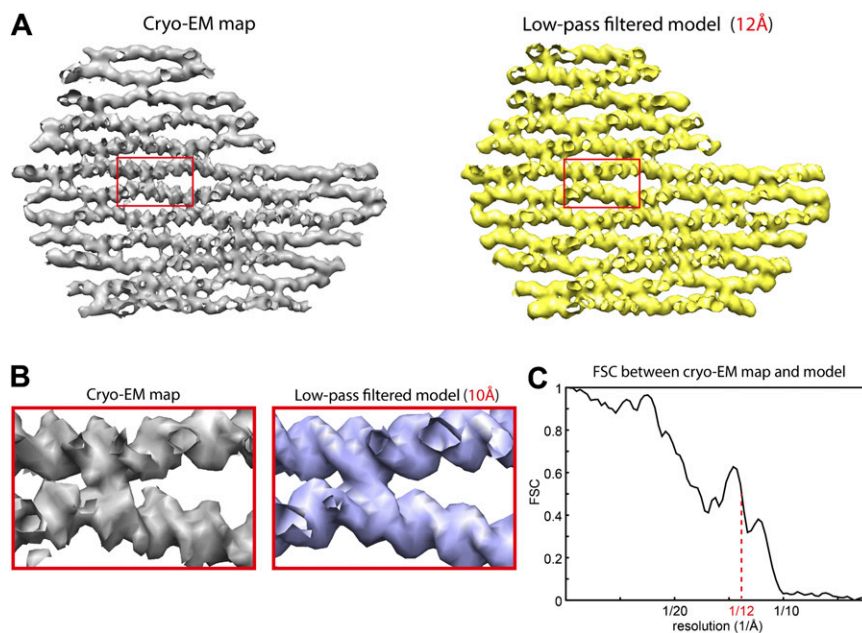
Fig. S6. Quality assessment of the pseudoatomic model. (*A*) Comparison of a slice (column 4) through the cryo-EM reconstruction and a 12-Å low-pass filtered map obtained from the pseudoatomic model. (*B*) As in *A*, but for a close-up of an area at the core of the object and a 10-Å low-pass filtered map obtained from the pseudoatomic model. (*C*) FSC between the cryo-EM map and the pseudoatomic model.
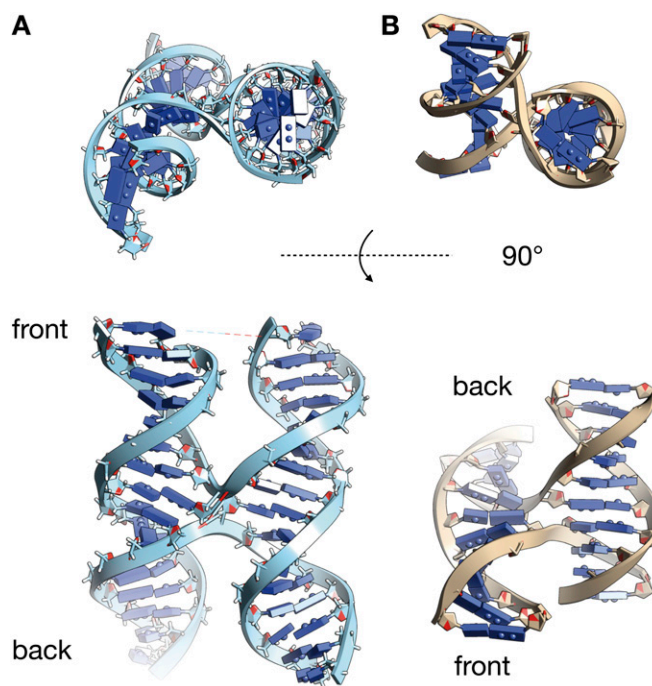
Fig. S7. Holliday junction conformation. (*A*) A typical Holliday junction in our structure (row 4, columns 4 and 5, base pairs 72–87). (*B*) Protein Data Bank ID code 1DCW. Both structures are depicted as ribbon-slab models. (*Upper*) The right helix in both junctions is pointing normally into the figure plane. (*Lower*) The right helix in both junctions is parallel to the figure plane.

Table S1. Sequence information

Start	End	Sequence	Length (nt)
0[79]	22[78]	CAAAGGGCGGGTGCCTCGCTCACTGCTTAATGTTGCATGCGGTCACGTTG	50
1[78]	23[77]	ATTGTTGTTCCGGCCAACCAGGGTGGTGCCAAGCGACAGGAAGCCGGA	48
3[43]	14[38]	TTTTTTTTTTTGGGTGAGACGGGCGAGTTTTTTTTTTAAAGGGTCGTGCCGAGGATCCCCGGGTTTTT	67
3[78]	21[74]	AGCGAAATCGCCTGGCCCTTGCCCCAGAGTAAAATAACATCACTT	45
4[69]	16[86]	AAAATCAGCCCCCGGCAGGCGAAAATCCTGACGCTGGTTGAGAGAGGG	48
5[62]	6[38]	GGGCCGTAAAGCACTAAATTTTTTTTTTTTCGGAACCGGAAAGCCGGCGATTTTT	54
6[100]	8[82]	TTTTTAGCGGTCCTTTTTTTTTTTTTGATGGTGGTTCAATAGCCCTTGGGC	51
7[38]	22[54]	TTTTTACGTGGCAACAGCTGAGAAGTTTTCCTTTTTTTTTTCAGTCACGACGTTGT	56
8[81]	32[82]	GCGCGCGGGGACGTGCTTCGCCGCTACAGCTTTCAATAGGAATTGCGG	48
9[90]	10[86]	AGGCGGTTTTTTTTTTTTTGCGTAGAGTTTTTTTTTTATAGGGTTGAGTAAAGAACTT	58
10[52]	13[53]	AACCTAAGGGTTTTTTTTTTAAGAAAGCGAAAGGTCACGCTAGCTCTTTTTTTTTTGAATTCGTAAT	67
10[85]	30[86]	GCGTTGAATGAGTGTAAAGTGTAATTGTTAAGGAAGATGATAATCATG	48
12[65]	3[77]	AACCCGCCGCGCCCGCTTTAATGAATCAGTTTGGCCTTATAAATCAAA	48
12[109]	32[106]	TTTAACTCGCGTCTTTTTTTTTTTGAAATGGATCACCATCAACTGTTTTTTTTTTTATAGCAAACAT	66
13[54]	51[45]	CAAAACGTTAAAACTAGCTTGAGAGATCTGGAGCTCATTGAATCCCCCTCGAATCG	56
14[61]	10[53]	ACTCTAAGCTGCATTCCAGTCGCGTGAACCGTCTATCAGGGCGATGTTTTTTTTTTGCCCACTAGGA	67
15[38]	33[53]	TTTTTTACCGGCGCGTAAACAACCCGAAATTTTTTAAAAATTCTGAGT	48
15[62]	1[77]	CAGTGTAGCGGAGCGGGCGCTAGGGCGAAAAACCAACAAGAGTCCACT	48
16[85]	44[86]	ATTTTATCCTCGTTCGTGCATCTGGTGTAGCACCAGCACTCAGAGCAA	48
16[111]	36[106]	TTTTTAACCAGAGGAATTTTTTTTTTTAAACGCTCCATCACCTCATTAG	48
18[64]	20[53]	GAGTAGAAGGTTGGGTAACGCCTTTTTTTTTTTTAGGGTGTTTTTATCCA	48
18[93]	37[81]	TCTTTGATTAGTAAGAGTCTGTGGGCGATCCCAGGCAACAATAACCCA	48
20[52]	56[54]	GCTGGCAGCTTTCGCGCGAGCAACACCGCTCCTGATTTAGAACCTGA	47
20[61]	2[43]	ATTACGAATCAGTGCAGAATCCTGATTGCCTTCACCAGGTCGAGGTATCACCCAAATCAAGTTTTTT	67
20[116]	41[106]	TTTTTGCAACGCTAGTTTGACATATCTTTTTTTTTTTGGTCAGTTGGCACCG	52
21[48]	59[53]	GCGATTAATAGCTCAACTGGAAGTCTTTTGATCTATTATACCATCCTAGTCCTG	54
21[75]	60[86]	GCTGGTAATATCCGAATTGAGCCAATTCTAGGTCAGGAAAAAGATGC	47
22[53]	52[54]	ATCGGCCGGCGGATTCAGTATTGGCAAAGAGATGATGATTAACAATAA	48
22[65]	5[61]	GACTTCTGGTCGGTACGCAGGCCACCATTTAGAGCTTGACGGCTAAAG	48
22[77]	63[73]	CCAGTTCTGAGAGCTGTTTAGCATTGCATCATTAGAGAAA	40
23[46]	64[54]	GCCGAAAGGGTACGGTGTCATGTTTTGCGGATGGCTTAGAGCTT	44
23[78]	64[82]	AAGGTGCGGGGTTGATTCGAAGGTTACTTTAGGAGCACTAACGTTTTA	48
23[102]	21[116]	TTAGGAGGCCCAAATTAACCGTTTTTTTTTTTTGCAGCCATTTTTTT	47
24[69]	4[70]	AATGTGATGGGATACTGCAGGTACGGCCAGTTTTTCTTCTTCACCGGC	48
24[77]	60[78]	CAACATAATAAAGCGAAGATAATTGCACGTGATGATGGCATCGGAAGT	48
24[89]	0[80]	GCCAGGGCGCCGGAAGCAAGCTAACTTTTTTTTTTTTCACATTAAGTGTTTTTTTTTTGACTCCAACGT	68
24[116]	42[106]	TTTTTTCAATCGTTGTACCAACCTAATTTTTTTTTTAACATCGCCATTAAGATTTTCGAGCGG	63
26[57]	24[78]	GTTGGTCATAGCTGTTTCCTGTGTGAAAAGCCTGTTTTAACCAT	44
26[77]	56[78]	TATAAGCAAAAGGGGAAGCCTTTTTTTAATATTTCAATCATATGCGGG	48
26[97]	25[116]	ACAAAATAATATACGAGCGTACTATGGTTTTTTTTTTTTGCTTTTGACGCTTTTT	55
27[90]	12[110]	CCATCACCAAAAACTCCGCTCACAATTCCACACTTTTTTT	40
28[80]	46[78]	GGCCAACAGATACGTGGTAATGCCGGGGAAGAAGG	35
28[105]	47[101]	CGATTAGTCTTTAATTTTTTTTTTTGCGCGAATATGATAACGGAACTGACGAGAAACACCAGTCAATA	68
30[61]	31[45]	CTATTTATGTCAATCCCTTCTGAAACAAGAGAATCGATCCTGAG	44
30[85]	51[73]	ATAAATCACAGACACCACATTCAACTAATGAT	32
31[27]	32[46]	TTTTTGGTCATTGGAATTTTTTTTTTTCGGTAATCGTAATATTTGTGCAATGCTT	55
31[46]	46[22]	AGTCTACAAAAAGAACTGTTGTGAATTACCTTATAGAAATTTTT	44
31[91]	28[106]	TTTTTGAATGGCTACCAGTAAATTGGCAGATTCACCATTTTTTTTTTGTCACA	53
32[45]	56[35]	TAGAACAATTACATAACAAACAATCATAATAGTACCGACAAAA	43
32[81]	51[93]	GATGAGAAAGGTAAATTGAAATCTACAAAAGAAGAGCAACACTATCAT	48
32[105]	58[110]	TATGTGAGTGAAGTTACAAGCCAACGATTTAACATAAATTGTAA	44
33[38]	45[41]	AATTATTTTTTTTTTAAATTCGCATTTCGGATTCACAGGCAATAGCATTAGG	52
33[54]	51[63]	AATTTAATCAGCTCATTAAATGTTTAATAAATATAAAGGAAT	42
35[27]	36[42]	TTTTTTAAATCATTCCTTTTTTTTTTGTGGGAACAAACTCAGGAAAATAGTAGTGAAAA	59
36[41]	65[53]	GGTACCCTGAAAGAGGTCTAAACCAATTATTTTTTTTTTTAATCAAGAT	48
36[93]	9[89]	AATGGTAGCGCCATATCGTAACAGAATCAGCACGTATAAG	40
36[105]	65[116]	ATAGACTTCAACCAGACCACCGCGCCTCCGGTATCTAACGAGCGTCT	47
37[58]	15[61]	GCAACATGAGGCGGTGACCGTAAGCGAGTACCACCA	36
37[82]	80[80]	GCAGCAGATTATCAAAAACAGATAGGCGGATTATACAAGACCTAAACTATATGTATCAATAG	62
37[122]	56[118]	CAAATATTTTTTTTTTTTTCAAACCCTCAATCATGCTGAACACCAGAAGAGGTTTAAAT	59
38[92]	7[100]	GAAAGAGAACAATGTTGGGAACCATCACGGATTAAAGTTGCAGCATTTTT	50
40[39]	21[47]	ATTTTTTTTTTTTTTAAATATGCTTTTTTTTTTTAACTAAAGGGATTTTTTTTTTTGTGCTGCAAG	64
40[61]	14[62]	TTGCTCTTCATTCCCATTTGGGCGGCACCGCGACGACAGTAAAACGCG	48

Start	End	Sequence	Length (nt)
41[107]	69[113]	TCAATAGATAATAAAGGCTTACAATAGCAGCGAATAAACAGCTTGATAATAAGTA	55
41[122]	58[118]	TTTGAGTCGAGCTTCAAAGCGAAATATCGCCTGAGGCTACTAAAGAAG	48
41[152]	60[146]	AACTTTTTTTTTAATTCGACAACTTTTAAAACATCGC	38
42[65]	18[65]	ATCAAAGCGGTATATTTTATATAACACCTCTTCGCTATCGGCCTTGCCT	49
42[105]	66[106]	AACTTTGAGGTGCAGGGATTTCTTAATAATTTTTAAAGTCAGATTTAT	48
43[22]	23[45]	TTTTTAAAATCAGGTCTTTGGCATCATTTTTTTTTTTATTCTACTGATTTTTTTTTTTTCGCACTCCA	66
43[98]	18[94]	CCCGAAACATTTCGGTAGATTTGCGCAACTATTACCGCTAGCAATACT	48
43[131]	65[151]	CGAACGTTATTAATCGTATTATAAACAACTGAATTTGTCGTCTTTCCAGACG	53
43[152]	56[146]	GTTTTTTTTTTTTTGAGTAACATTTACCTTTTGAGGCG	38
44[85]	71[73]	TTATTCGGAAACAGTTAGATTAAGACGCTGTTATATAATTTAATGGGG	48
45[42]	62[40]	AAGGGTGTTTGGATATAGATAAATTTACGAGCATGTTTTTTTTTTTAGAAACCAATCAACGGGTAT	66
45[58]	26[58]	CATATCCAAAAGAAATTAGCAACGCAAGGAGTTAAATCTAAATT	44
45[142]	67[137]	AGATCATTTTTTTTCCATTACGCATAACGACAATGTAGAAAGGAG	44
45[152]	54[138]	ACATTTTTTTTTTTCGGGAGAAACTCATTACCGTAATCTTGACAAGAACTGACCTTGTACAG	62
46[77]	24[70]	CTTGAGATGGTTTAAATTACCTTATTTCAAAATTAAGCTA	40
47[22]	33[37]	TTTTTACGAGACAAAATTCCTCATATTTTTTTTTTTATTTTA	42
47[94]	28[81]	AAAACGAGTAGCCGGAGAGTTCTAGCGAAAAGCCTAAAAGGGACATTCT	49
47[102]	17[111]	TATGACCCTGAAATCGGTCTGGCCTTACCTACATTTGACGAGAGCGGGAGCTATTTTT	58
47[114]	71[109]	TAACCTTCCCTTAGAATCCTTGCCAATCGCATATTTTAAGTACC	44
47[130]	57[141]	AATCGTCCGGATATAATAACGGACTGACCAGACGGTCAGTTACT	44
47[152]	47[129]	CAATTTTTTTTTTTATCAACGTAACAAAGCTGCTCATTCAGTA	42
48[34]	30[27]	CTTTAAACTTTTTTTTTTTAGTTCGCGATTTTGGCTATCATTTTT	44
48[61]	26[78]	ACGCCAACCTGAAAGCGTAAGAAGATAGAACATATGTACCCCGGTTTG	48
48[127]	50[110]	TTTTTAGGTAGAAAGATTCATCAGTACCAGACGACGATTTTTTTTTTTTAAAAAC	54
50[109]	31[90]	CAAAATAGCGAGAGGCTTTTGCGTTAATAATAGGAATAATA	41
51[46]	48[35]	TCGACTGGATAGCGTCCATTTTTTTTTTTTATACTGCGAAATG	41
51[64]	12[66]	TACGAGGCCAGATACAAGGACGTTGAGAGGGTTAAAGATTCAAATATTAGCTCATTGCTGGC	62
51[74]	48[62]	AGTAAGTTTTGCCAGAGGGGGTAATAGTAATACCAGTCTA	40
51[94]	26[98]	AACCCTCGTTTTGAGATTAACGAACTATTCAACCCAGTCAAATTATTT	48
52[53]	54[42]	TTTATCAAAATCATAGGTCTTTTTTTTTTTTTGAGAGACTACCTATAAGG	48
52[65]	22[66]	GTTTTAGTATTACCTGAGAAAATTATAACAGAGGGTGCCACGTGAGGG	48
52[101]	23[101]	AACATACAGTATAAAAATCGCGAATTGCGTAAAATACCATCTAAAGATGGAAATTCGCCA	60
52[125]	49[127]	TAATTTTGCTTCTGTGAATAAGGCTTGCCCAACATTATTACTTTTT	46
53[120]	45[141]	GAACGCGATAGGCTGGCGCTATTAGGAACCGAATTCGCCTGAATATACAGTAAC	54
54[41]	74[38]	CGAACGCAATAAGTTACCTTTGGGAATTAGAGCCTTAGCGTTTGCCATTTTT	52
54[57]	30[62]	CGAAAGCCTGCAATAGTGTTCATTTGATTTCAACTGTGTAGGAG	44
54[137]	73[148]	ACTGATATAAGTATATTTTTTTTTTTGCCCGGAATAGGTAGGCTGAGTTTTT	51
55[38]	34[27]	GATCAAGAAAAATGATTTTTTTTTTTCCATATGAATAATACATCCAATTTTT	51
56[53]	72[32]	ATATAATACTAGAATGTGATAATTTTAACCCAAAGACAAAATTTTTTTTTTTGGGACCGACTTGAGTTTTT	70
56[77]	67[65]	CATTTTAAAGTACACAGCGATTCCCATGTATACCGAAGCCCTTTTTGA	48
56[93]	27[89]	GTAATTAATAAAGACAGAGGCGATAAAGCTTAATACTTCG	40
56[117]	81[105]	CGCCATCTCAACAGTTTCAAATAAGACAAAAAGCACCACGGAATAAT	48
56[145]	53[151]	CAACTTTGAAAGAGGTTTTTTTTTTTACGATGAACGGTCATCAAGA	46
57[35]	42[22]	GGTAAAGTAATTCGCTAATGCAGAACGCGCCTTTTTTTTTTTTGTTATCAACATATACTTCAATCATTTTT	71
57[142]	68[136]	TAACGAAGGCACAGCCCTCATAGTTTTTTTTTTTTTAGCCCCACAAG	46
58[109]	65[97]	GAATACGTACAAACAGCAAGAAACAATGAACCCTGAACTCACGTTGTA	48
58[117]	81[119]	AGGCAAGTCGAAATGAGGTTTAGCGGATAATAGCGGGGGAAACGCA	46
58[125]	47[113]	AACGAACTTTTTCAAATTGAGACGTCAGATGATTGCTTTGAATACCAA	48
59[54]	81[55]	AACATGTTCATGTCCAGACTCATTTTAATAACGGTCACCGTCCGACATTC	50
60[77]	66[62]	CACCCTGTATCGGTAGGCTCCATTAGACGGTGTTTAACGTCAAAAATG	48
60[85]	70[82]	GGGATCCGAGGGTATTGACCCCACGGAGATCCCTCA	36
60[89]	24[90]	TTTAAGAGGAATATTCCTAATGAAAAGAACGAACATGGGCGCCCTGTA	48
60[133]	64[146]	GATATAGATTTTGCAATCCTTTGATTTAGAAGTATTAGACTTTACATTAGTA	52
60[145]	57[151]	CCAAACGGGTAAAATTTTTTTTTTTTACGTAATGCCACTGCCGGAAC	46
61[98]	38[93]	GGTGAAGTTAAAGGGAATCATTGGAAGCAAGATTAGAGAATCAACAGTT	49
63[70]	20[62]	GCGTACCTTTTGAAATATTCTAAATATAATGCTGAACTCAAACT	44
63[74]	67[89]	GCCGTTGAACCTCCCAGCTACAATTTTATCCGATTTTTGAGAATTAAC	48
64[53]	68[38]	GAAGCCGTACCGCATTCCAAGAATAATCGGTAAGCAGATAGCCTTTTT	48
64[81]	69[93]	GCTTTATTTTCAAAAAAAATTATCAGCAGCTATCTCCGTAACACTGAGT	48
64[145]	61[151]	AATTTCAACAGTTTCTTTTTTTTTTTAGCGGAGTGAGAAACAACAAC	46
65[54]	67[55]	TAGCAGCCTTTACAGTTTTTTTTTTTAGAGAATAACATA	38
65[98]	36[94]	CCAACGTCTAAGAACGCGAGGCAACTAATAACTCCAACGCGAACGACA	48

Start	End	Sequence	Length (nt)
65[117]	58[126]	TTCGCCATATTAGGGTAATTGAGCGCTTAAGCCCAATACCGATAA	45
66[61]	37[57]	AAAATAGTTGCTATCCTTATCACTCATCGAATAATATCGTCAGAAGCAATATAACT	56
66[105]	60[90]	CCCAATCCAAATAAGAAACTGAATCTAAAATCTCCATCGTAGCCGCTT	48
66[121]	37[121]	CACAGAGCCTAAGGAATTAGCAAATCTTCGGTCGGTTTTAATAAGAAACCCT	52
67[56]	45[57]	AAAACAGGAAGAAAAGCTGTCTTTATAAACAACAAGAAAATAATAAGAAC	50
67[66]	40[62]	AGCGCAAAAGGAGCTTTGCACCCGACTTGCGGGAGGTTTTAATTGCAA	48
67[90]	56[94]	TGAACAATAGCAATTTGCTTTCACTCATCTGCAACGGCAT	40
67[138]	66[122]	AGATAAGTAACTTTTTTTTTTTGATCTAAAGTTTTAGTTACAAAATAAA	48
68[135]	41[121]	AATTGAGTAATATCAGAACAACTAAATTTGCCCTGTATGGAGATATAGCA	50
69[38]	54[58]	TTTTTGAACACAGGGATAGCAAGCCCCCACCACCCGACGACAACCGAC	48
69[94]	47[93]	TTAACCGCCATTGTATCACATCTTCTATTCTTACGCGATAGCTACATA	48
69[114]	52[126]	CAACGCCTGTAGCAGTACTCAGCCGCGACCGAAAACTTTAGGGCTTAT	48
70[81]	79[77]	GATAAGACTCATAGACGGATATTCATGAGCCGCCGCCAGCATCGCCTC	48
71[74]	76[86]	CATGATACCGCCACGCACCATTACCATTAGTTTCATCGTAAACAGTGT	48
71[110]	75[117]	AGGTACCGCCACCAATGAAACCATCGAAGTTTGCCCTATT	40
71[122]	43[130]	GCCGTCGAGAGGGTCAGGCGCATGCTCCATATCATAAGTGAGGAAGGCGGAACAGCC	57
72[148]	71[121]	TTTTTACTCCTCAATTTTTTTTTTTTAAGCAGTAGCGACAGAATCATAGCAGCATTAGGATGT	63
73[32]	55[37]	TTTTTCCAAGAAGGAATTTTTTTTTTTACCGAGGATTAAATAAGAATTTTTTTTTTTTAAACACCG	64
73[62]	52[66]	ATGTGAATTAAATACCCAACCAGCGCTCCGGCTTAGGTTGGGAGAAGA	48
73[70]	63[69]	TACCTCAGAGAATAGGAAATACCAAGCTTTAATTCAGCAGCGGAACAA	48
74[89]	52[102]	GTCAAGGCCGCGTAGAAACTTATTACTTGTCACAAAATGCTGATGCAAATAA	52
75[38]	77[61]	TTTTTTTCTTTTCATAATCCCTTGATATTTTTTTTTTTTCACAAACAAATA	50
75[98]	61[97]	TGCCTATTAGCAAAGAAACGTCACCCTCAGCGTCACCAACTAAAACGA	48
75[118]	78[106]	ATGAGTGTACAGAGCCACTTTTTTTTTTTTCACCCTCAGAGCCG	42
75[132]	60[134]	AAGTAGAGAAGGACCGTAATGTATCACCTTCCACAGACCAACCTAGTTGCGCCC	54
76[85]	75[97]	GCCTTGTCAGAGCCGCGCACCCTCAGAACCGACCAGAACCC	40
77[62]	80[66]	AAACGATTGGAAAATCACGGTTGAGGAACCGATTGAGGGAGGTATGGT	48
77[84]	81[101]	GAAAGCGCAGTCCGGGGTCATAATGCCCCACCACCAACATAAAGGTGGCA	50
77[122]	75[131]	CATACATGGCTTTTTTTTTTTTTTTGATGATACAGTCTGAAACATGA	46
78[105]	74[90]	CCCCACCCTCTGGTAATAAGTTTTAATCTGAATTTCAGACTGTAGCGC	48
79[56]	73[69]	CAGGTCAGACCGGAACTGACAGGACGGAACCACATTAAAGCACCAG	46
79[78]	73[61]	CCAGTAACAGGAGCCACCTCCTCATTGGTCATAGCCCCCTTAAGCAAA	48
80[65]	42[66]	TTAAAGAACTTTTGAAATCGCGAAACCGAGCCAGAAAGACAGCAATTC	48
80[79]	77[83]	AAAATTCAGAAGGTAAAAATTATTTGCCCGTAGCATTTTCAAAGCCAGAATG	52
81[102]	43[97]	ACAGTTTATTGCAGTATGGTTAATTTTCGCCTGAACGCCAACTACAGAGGTTATCATCAG	60
81[106]	77[121]	ATAAAATTTTGCTCTTTCGGAACTTTAGCGTACCGTTCCAGTAAGCGT	48

The table lists the sequences of the 163 "staple" DNA oligonucleotides that form the object in addition to the M13mp18 scaffold DNA strand. "Start" and "End" refer to the location of 5′ and 3′ termini in the strand routing scheme (Fig. S1). The first number indicates the helix number; the second number (between square brackets) indicates the nt position within that helix.

Movie S1.   The reconstructed cryo-EM density map (gray) is shown in gray, the pseudoatomic model in blue (scaffold strand) and red (staple strands).

Movie S1